Iranian Journal of Mathematical chemistry

IJMC

DOI: 10.22052/IJMC.2026.258174.2107
Vol. 17, No. 4, 2026, pp. 339-362
Research Paper

On the Analytic Solution for the Surface Concentration and Impedance in AC Experiments at Circular Disk Electrodes

Stanley Pons[1⋆] and Tibor K. Pogány[2]

[1]Department of Chemistry, University of Utah, Salt Lake City, UT 84112, USA, and Pons(EI), 14, rue Eugene Giraud, 06560 Valbonne, France.
[2]Institute of Applied Mathematics, Óbuda University, 1034 Budapest, Bécsi út 96/b, Hungary, and Faculty of Maritime Studies, University of Rijeka, 51000 Rijeka, Studentska 2, Croatia.

Keywords:
Electrochemical impedance, Modified Struve function, Diffusion equation

AMS Subject Classification (2020):
78A57; 33C10; 33E20.

Article History:
Received: 22 December 2025,
Accepted: 7 August 2026

Abstract

This work presents an exact analytical solution for the time-dependent concentration of an electroactive species at a circular disk electrode under a periodic flux. The solution is derived using a complete Laplace transform treatment of the diffusion equation, yielding a closed-form expression for the steady state and an exact analytical representation for the transient regime. The steady-state solution is expressed in terms of a modified Struve function of the second kind, $\mathbf{M}_1(z)$, thereby eliminating the need for numerical integration of Bessel functions. The transient solution, given in terms of Fresnel integrals and modified Bessel functions, explicitly captures the temporal behavior from $t = 0$ to steady state. Critically, this work demonstrates that the transient component, previously treated as a correction or simply ignored, contains independent information about the diffusion coefficient D and electrode radius a. This information can be extracted from a single experimental measurement. The complex impedance components, directly derived from the steady-state solution, provide an alternative to traditional integral-based formulations. The analytical framework introduced here enables rapid parameter extraction, sensitivity analysis, and optimal experimental design, all of which are inaccessible to purely numerical approaches.

© 2026 University of Kashan Press. All rights reserved.

*Corresponding author
E-mail addresses: bpons@laposte.net (S. Pons), tibor.poganj@uniri.hr (T. K. Pogány)
Academic Editor: Abbas Saadatmandi

1 Introduction

The electrochemical impedance of disk electrodes has been widely studied due to their extensive applications in amperometric sensors, battery diagnostics, and corrosion monitoring. The canonical problem 'semi-infinite diffusion to a circular disk electrode embedded in an insulating plane' was first analytically addressed by Fleischmann et al. [1], who derived integral expressions for the steady-state concentration using discontinuous Bessel function integrals and Neumann's integral theorem. This approach has since become the standard for analyzing disk electrodes and has been employed in numerous electrochemical impedance spectroscopy (EIS) experiments [2–6], as well as serving as a benchmark for numerical simulations [2, 3, 7–12].

However, the integral-based formulation has notable limitations. The concentration and impedance are expressed as semi-infinite integrals of Bessel functions, which requires numerical evaluation for each frequency and geometry. Furthermore, the transient response (the evolution of the concentration from the moment the perturbation is applied) has received relatively little attention. Existing treatments either focus solely on the periodic steady state [13, 14] or rely on numerical approximations for time-dependent behavior [7–9, 11]. Critically, the transient response contains readily accessible information about the diffusion coefficient and electrode geometry, which is less straightforward to obtain via conventional frequency-domain measurements.

Currently, several gaps remain in this field. First, no fully closed-form expression exists for the complete time-dependent concentration at a disk electrode under periodic flux. While the steady-state component can be expressed in closed form via a modified Struve function, the transient component retains an integral representation that has resisted reduction to named special functions. Prior literature has relied on integral representations or numerical solutions that, unlike the present work, lack the analytical structure necessary for rapid parameter extraction, sensitivity analysis, or experimental optimization. Second, the relationship between the transient and steady-state components remains undefined. The transient is typically regarded as an experimental artifact to be minimized (either by waiting for steady-state conditions or by optimizing experiments for this regime, *e.g.*, in EIS experiments) rather than as a source of additional information. Consequently, the information content of the transient, which includes the diffusion coefficient and electrode radius, remains largely untapped. Finally, existing analytical treatments do not provide a unified framework that simultaneously captures the transient response, the periodic steady-state, and the complex impedance from a single Laplace transform solution. Instead, the impedance is often derived separately, frequently requiring distinct mathematical tools.

This paper aims to fully quantify all contributions to the average surface concentration predicted by the diffusion equation system in its complete form. The derived concentrations, in their analytic forms, are applicable to several electroanalytical techniques, including EIS. However, the application of these solutions to specific experimental techniques falls beyond the scope of this work and will not be detailed here.

This paper addresses these challenges by presenting a closed-form analytical solution derived via a complete Laplace transform treatment of the diffusion equation (see Section 2 for details). The key contributions are:

- The steady-state solution is expressed in terms of a single modified Struve function of the second kind $\mathbf{M}_1(z)$:

$$\langle C\rangle_1 = \frac{Q}{\sqrt{2D\omega}}\left[(\sin\omega t - \cos\omega t) - \Re\left\{e^{i\omega t}\frac{\mathbf{M}_1((1+i)a\sqrt{2\omega/D})}{a\sqrt{2\omega/D}}\right\}\right], \tag{1}$$

where a, ω, Q, and D are the electrode radius, angular frequency, flux amplitude, and diffu-

sion coefficient, respectively. The argument of this Struve function is complex, and a recent discussion [15] of its structure and properties was useful in extracting and understanding the behavior of the full solution described herein. This analytical solution replaces previous integral representations and provides insight into the underlying diffusional physics, as discussed in more detail below.

- A previously unavailable analytical solution is derived for the transient concentration, $\langle C\rangle_2$, expressed in terms of Fresnel integrals and modified Bessel functions:

$$\begin{aligned}\langle C\rangle_2 = \frac{Q}{\sqrt{2D\omega}}\left\{\left[\cos(\omega t)-\sin(\omega t)\right]+\frac{2\sqrt{2}}{\sqrt{\pi}}\left[\sin(\omega t)\,C\left(\sqrt{\omega t}\right)-\cos(\omega t)\,S\left(\sqrt{\omega t}\right)\right]\right\}\\ -\frac{Q}{\sqrt{\pi D}}\int_t^\infty \frac{\sin\omega(\tau-t)}{\sqrt{\tau}}\exp\left(\frac{-a^2}{2D\tau}\right)\left[I_0\Big(\frac{a^2}{2D\tau}\Big)-I_1\Big(\frac{a^2}{2D\tau}\Big)\right]\mathrm{d}\tau.\end{aligned} \tag{2}$$

This solution explicitly captures the concentration decay response following flux application, from $t = 0$ to steady-state, revealing unique $t^{3/2}$ short-time behavior due to radial diffusion at the disk edge.

- The procedure for extracting both the real and imaginary impedance components without numerical integration is detailed. Unlike prior work, which required separate derivations for concentration and impedance, the Laplace transform approach presented here yields both impedance terms simultaneously.
- It is demonstrated that the total measured concentration, $\langle C\rangle_{\text{total}} = \langle C\rangle = \langle C\rangle_1 + \langle C\rangle_2$, contains separable contributions: the steady-state component, $\langle C\rangle_1$, encodes the complex impedance, while the transient component, $\langle C\rangle_2$, encodes the diffusion coefficient and electrode radius. This separation 'impossible in integral-based formulations' enables the extraction of up to four independent parameters (D, a, Q, ω) from a single time-domain measurement.
- The analytical structure of the solution enables convenient parameter sensitivity analysis and can be used to aid experimental design for specific problems. Identified below are the conditions 'microelectrodes ($a \sim 1\,\mu$m), kHz frequencies, and sub-millisecond observation times' where the transient contributes maximally to the total signal, thus indicating regions of highest accuracy for extracting diffusion parameters.

The article describes the mathematics of the new solution and the formalism for determining the components of the complex impedance. Comments on problem stability are followed by a parameter sensitivity analysis. Full mathematical details are provided in the appendix.

2 Mathematical formulation and solution

2.1 The diffusion equation system for the circular disk electrode

First, consider the diffusion-controlled transport of an electroactive species to a circular disk electrode of radius a embedded in an otherwise insulating planar boundary. The electrode is located in the plane $z = 0$ and occupies the region $0 \le r \le a$, where r is the radial coordinate measured from the disk center. The electrolyte occupies the semi-infinite half-space $z > 0$.

The concentration $C(r, z, t)$ of the electroactive species satisfies Fick's second law in cylindrical coordinates:

$$\frac{1}{D}\frac{\partial C}{\partial t} = \frac{\partial^2 C}{\partial r^2}+\frac{1}{r}\frac{\partial C}{\partial r}+\frac{\partial^2 C}{\partial z^2}, \quad r, z, t \ge 0, \tag{3}$$

where D is the diffusion coefficient. The system is initially at equilibrium:

$$C(r, z, 0) = 0, \quad r, z \ge 0. \tag{4}$$

A periodic flux source of amplitude Q and angular frequency ω is applied to the steady-state componentectrode surface at $t = 0$:

$$D \left.\frac{\partial C}{\partial z}\right|_{z=0} = \begin{cases} -Q\sin(\omega t), & 0 \le r < a,\ t > 0, \\ 0, & r > a,\ z = 0,\ t > 0. \end{cases} \tag{5}$$

The surrounding plane is insulating. Far from the electrode, the concentration decays to zero:

$$\lim_{r\to\infty} C(r,z,t) = 0, \quad \lim_{z\to\infty} C(r,z,t) = 0. \tag{6}$$

The solution to Eqs. (3)–(6), and the conversion of C to $\langle C\rangle$ (the measured quantity), is obtained via the Laplace transform of this parabolic system of equations. This process requires extensive use of the properties of Bessel and Bessel-type functions, as well as Feynman integration [16] for such functions. The details are presented in Appendix and summarized here.

The average surface concentration $\langle C\rangle$ comprises two components: $\langle C\rangle = \langle C\rangle_1 + \langle C\rangle_2$:

2.2 The steady-state component $\langle C\rangle_1$

The steady-state component, $\langle C\rangle_1$, represents the oscillatory response that persists after all initial transients have decayed. It arises from singular poles in the Laplace space representation of the system:

$$\langle C\rangle_1 = \frac{Q}{\sqrt{2D\omega}}\left[(\sin\omega t - \cos\omega t) - \Re\left\{e^{i\omega t}\frac{\mathbf{M}_1((1+i)\beta)}{\beta}\right\}\right], \tag{7}$$

where $\beta = a\sqrt{2\omega/D}$ is the dimensionless frequency parameter used in Equation (1).

The complex argument, $(1+i)\beta$, in Equation (7) carries both the amplitude and phase information of the steady-state response. The Struve function, $\mathbf{M}_1$, is functionally equivalent to the semi-infinite Bessel function integrals present in previous formulations [1–3].

2.3 The transient component $\langle C\rangle_2$

The transient component, $\langle C\rangle_2$, captures the concentration transition from the initial equilibrium state at $t = 0$ to the eventual steady-state oscillation. It arises from the branch-cut singularity in the Laplace space equations of the system (see Appendix and is given by Equation (2), rewritten here for convenience:

$$\begin{aligned} \langle C\rangle_2 = {} & \frac{Q}{\sqrt{2D\omega}}\left\{\left[\cos(\omega t) - \sin(\omega t)\right] + \frac{2\sqrt{2}}{\sqrt{\pi}}\left[\sin(\omega t)\, C\left(\sqrt{\omega t}\right) - \cos(\omega t)\, S\left(\sqrt{\omega t}\right)\right]\right\} \\ & - \frac{Q}{\sqrt{\pi D}}\int_t^\infty \frac{\sin\omega(\tau - t)}{\sqrt{\tau}}\exp\left(\frac{-a^2}{2D\tau}\right)\left[I_0\left(\frac{a^2}{2D\tau}\right) - I_1\left(\frac{a^2}{2D\tau}\right)\right]\mathrm{d}\tau, \end{aligned} \tag{8}$$

where $S(x)$ and $C(x)$ are the non-normalized Fresnel integrals:

$$S(x) = \int_0^x \sin\left(\frac{\pi u^2}{2}\right)du, \quad C(x) = \int_0^x \cos\left(\frac{\pi u^2}{2}\right)du, \tag{9}$$

and $I_\nu(x)$ are the modified Bessel functions of the first kind.

2.4 Surface concentration dynamics

The total average surface concentration, $\langle C\rangle = \langle C\rangle_1 + \langle C\rangle_2$, describes the complete behavior of the electroactive species. In electroanalytical techniques, $\langle C\rangle$ is the physically measurable quantity, manifesting as the voltage or current measured during the experiment.

The steady-state response, $\langle C\rangle_1$, is the forced oscillatory response that would exist if the AC perturbation had been applied for all time ($t \to -\infty$). This component contains both the real and imaginary parts of the complex impedance through the Struve function component, $\mathbf{M}_1((1+i)\beta)$, as fully discussed in Section 3. This mathematical structure is inaccessible in integral-based or purely numerical approaches.

The transient component, $\langle C\rangle_2$, is the causal correction that ensures the total concentration vanishes at $t = 0$. Its parameters 'the diffusion coefficient D and electrode radius a' independently determine the timescale of the transient response. Understanding these properties is critical for experimental design and parameter extraction. Define a convenient diffusion time constant, $\tau_D = a^2/D$, e.g., as the characteristic time for a diffusing species to travel a distance of one electrode radius. The transient, $\langle C\rangle_2$, exhibits a characteristic evolution that can be understood through three distinct time regimes:

(1) **Short-time behavior** ($t \ll 1/\omega$, $t \ll \tau_D$):
The Fresnel terms in Equation (8) dominate, yielding:

$$\langle C\rangle_2 \propto (\omega t)^{3/2}. \tag{10}$$

This $t^{3/2}$ scaling is a direct consequence of the finite disk geometry, and reflects the combined effects of planar diffusion and edge contributions due to the finite disk size. This $t^{3/2}$ growth is characteristic of all disk electrodes and distinguishes them from infinite planar electrodes, where $C \propto t^{1/2}$ behavior (Cottrell behavior) is observed.

(2) **Intermediate behavior** ($1/\omega \ll t \ll \tau_D$):
The system behaves as if on an infinite plane, with the amplitude decaying as:

$$\langle C\rangle_2 \propto \frac{1}{\sqrt{t}}. \tag{11}$$

This is the classical Cottrell behavior for planar diffusion.

(3) **Long-time behavior** ($t \gg \tau_D$):
The finite disk geometry becomes apparent through the Bessel integral in Equation (8), which introduces an exponential cutoff:

$$\langle C\rangle_2 \propto e^{-Dt/a^2}. \tag{12}$$

The Bessel integral in the second part of $\langle C\rangle_2$ vanishes exponentially with t, while the Fresnel expression in the first part vanishes algebraically and more slowly as $1/\sqrt{t}$. The crossover between the $1/\sqrt{t}$ and exponential decay occurs at the diffusion time constant $\tau_D = a^2/D$.

Figure 1 displays time evolution profiles for the average measured concentration and its steady-state and transient components for a typical electrochemical experiment. One dotted line marks the location of $1/\omega$, the period of the applied oscillating flux, while a second mark a^2/D, the diffusion time across the electrode surface. Stability, response, and parametric sensitivity are discussed for this plot in Sections 5 and 6.

Note: The geometric form factor, represented by the Struve function of decreasing amplitude specific to the disk structure, is particularly interesting. As Levine [17] notes, it is rare to have

solutions to the diffusion equation with combinations of cylinder functions with arguments comprising the aperture size (i.e., a) and the transport term (i.e., D). Such combinations are typically found only in asymptotic developments for wave-scattering problems, suggesting diffraction-like wave effects at the disk edge.

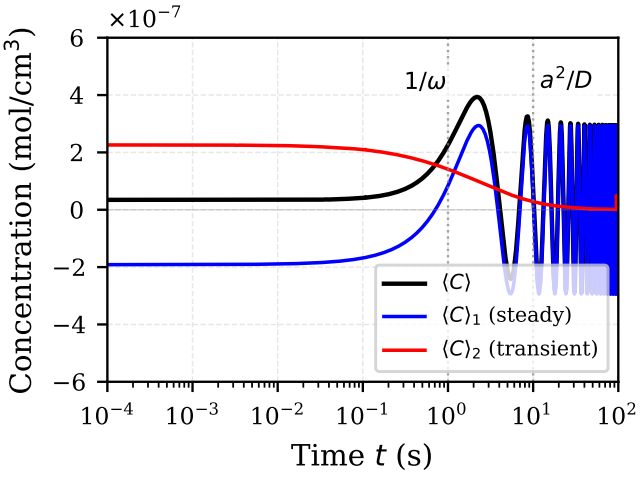


Figure 1: Time evolution of $\langle C\rangle$ (black), $\langle C\rangle_1$ (blue, steady-state), and $\langle C\rangle_2$ (red, transient). Vertical lines indicate $1/\omega$ and a^2/D. Parameters: $Q = 10^{-9}$ mol/(cm^2 s), $D = 10^{-5}$ cm^2/s, $a = 0.01$ cm, $\omega = 1$ rad/s.

3 The electrochemical AC impedance

The mass transfer impedance, Z_{mt}, in the frequency domain is obtained directly from the Laplace representation of the concentration response of the two poles at $s = \pm i\omega$. The Struve function form of the Laplace concentration (Equation (25)),

$$\langle \bar{C}\rangle = \frac{2Q\omega}{D(s^2+\omega^2)}\left\{\frac{1}{2\sqrt{\frac{s}{D}}} + \frac{\mathbf{M}_1\left(2a\sqrt{\frac{s}{D}}\right)}{2a\frac{s}{D}}\right\},$$

is divided by the Laplace transform of the applied AC flux density, $Q\sin\omega t$, and the active surface area to obtain the Laplace space mass transport impedance function, Z_{mt}:

$$\bar{Z}_{mt} = \frac{1}{\pi D a^2}\left\{\frac{1}{\sqrt{\frac{s}{D}}} + \frac{\mathbf{M}_1\left(2a\sqrt{\frac{s}{D}}\right)}{a\frac{s}{D}}\right\}.$$

Considering the causality and analyticity of the function over the circular region of interest, conversion from the Laplace to the Fourier frequency domain is immediate with the substitution of s by $i\omega$, which gives

$$Z_{mt} = \frac{1}{\pi D a^2}\left\{\frac{1}{\sqrt{\frac{i\omega}{D}}} + \frac{\mathbf{M}_1\left(2a\sqrt{\frac{i\omega}{D}}\right)}{a\frac{i\omega}{D}}\right\} = \frac{1}{\pi D a\sqrt{iz}}\left\{1 + \frac{\mathbf{M}_1\left(2\sqrt{iz}\right)}{\sqrt{iz}}\right\},$$

upon assigning a dimensionless frequency $z = a^2\omega/D$. Writing

$$\Phi_{4,A}(z) = \Re\left\{\frac{1}{\sqrt{iz}}\left[1 + \frac{\mathbf{M}_1\left(2\sqrt{iz}\right)}{\sqrt{iz}}\right]\right\}, \tag{13}$$

$$\Phi_{5,A}(z) = \Im\left\{\frac{1}{\sqrt{iz}}\left[1 + \frac{\mathbf{M}_1\left(2\sqrt{iz}\right)}{\sqrt{iz}}\right]\right\}, \tag{14}$$

for the real (in-phase) and imaginary (quadrature) components of the impedance, respectively, the total complex concentration impedance is then

$$Z_C = \frac{1}{\pi Da}\left(\Phi_{4,A}(z) + i\,\Phi_{5,A}(z)\right).$$

Using the Butler-Volmer polarization equation, as in [1], cast in terms of the average surface concentrations of the couple in the electrode reaction $\mathrm{Ox} + \mathrm{e}^- \rightleftharpoons \mathrm{Red}$, $\langle C\rangle_{1,O}$ and $\langle C\rangle_{1,R}$ from Equation (7),

$$\begin{aligned} Q = \frac{i_0}{nF}\Bigg\{&\left(\frac{C_R^s - \langle C\rangle_{1,R}}{C_R^\infty}\right)\exp\left(\frac{(1-\alpha)(\eta+\Delta\eta)nF}{RT}\right) \\ &- \left(\frac{C_O^s - \langle C\rangle_{1,O}}{C_O^\infty}\right)\exp\left(\frac{-\alpha(\eta+\Delta\eta)nF}{RT}\right)\Bigg\}, \end{aligned}$$

may be linearized after accounting for the usual required steady periodic state EIS experimental conditions, *e.g.*, electrolysis at the reversible potential of the reaction with small-amplitude AC current, equal diffusion coefficients D_O, D_R and equal DC surface and bulk concentrations ($C_R^s = C_O^s = C_O^\infty = C_R^\infty = C^\infty$). Subsequent derivation of the real and imaginary components of the total AC impedance, Z, in the original work gave the semi-analytical forms

$$\Re(Z) = \frac{RT}{\pi nFi_0a^2} + \frac{4RT}{\pi n^2F^2D^{1/2}\omega^{1/2}a^2C^\infty}\cdot\Phi_4\left(\frac{\omega a^2}{D}\right),$$

$$\Im(Z) = \frac{4RT}{\pi n^2F^2D^{1/2}\omega^{1/2}a^2C^\infty}\cdot\Phi_5\left(\frac{\omega a^2}{D}\right),$$

where the variables

$$\Phi_4\left(\frac{\omega a^2}{D}\right) = \Phi_4(z) = \int_0^\infty J_1^2(\beta\sqrt{z})\frac{\cos\left(\frac{1}{2}\arctan\left(\frac{1}{\beta^2}\right)\right)}{\beta\left(1+\beta^4\right)^{1/4}}\,\mathrm{d}\beta,$$

$$\Phi_5\left(\frac{\omega a^2}{D}\right) = \Phi_5(z) = \int_0^\infty J_1^2(\beta\sqrt{z})\frac{\sin\left(\frac{1}{2}\arctan\left(\frac{1}{\beta^2}\right)\right)}{\beta\left(1+\beta^4\right)^{1/4}}\,\mathrm{d}\beta.$$

The last two relations combine and rearrange into the dimensionless forms

$$\frac{\pi n^2F^2DaC^\infty}{2RT}\Re(Z) - \frac{nFDC^\infty}{2ai_0} = 2\left(\frac{D}{\omega a^2}\right)^{\frac{1}{2}}\Phi_4\left(\frac{\omega a^2}{D}\right) = \frac{2}{\sqrt{z}}\Phi_4(z), \tag{15}$$

$$\frac{\pi n^2F^2DaC^\infty}{2RT}\Im(Z) = 2\left(\frac{D}{\omega a^2}\right)^{\frac{1}{2}}\Phi_5\left(\frac{\omega a^2}{D}\right) = \frac{2}{\sqrt{z}}\Phi_5(z). \tag{16}$$

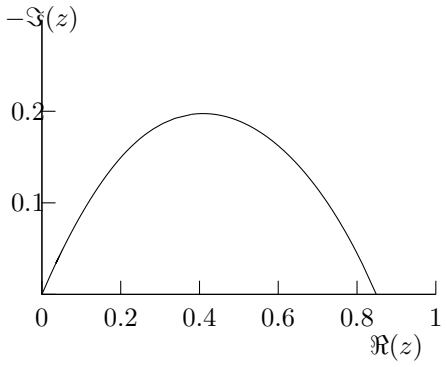


Figure 2: Bode plot of the real and complex components of the AC mass transport impedance given in Equations (13) and (14).

The right-hand terms of Equations (15) and (16) are equivalent to the new analytic values in Equations (13) and (14), respectively, since they are sourced from the same complex two-pole contribution of Equation (26). The final analytic quantities of interest are the dimensionless mass transport impedance forms

$$\frac{\pi n^2 F^2 DaC^\infty}{2RT}\,\Re(Z) - \frac{nFDC^\infty}{2ai_0} = \Re\left\{\frac{1}{\sqrt{iz}}\left[1+\frac{\mathbf{M}_1\left(2\sqrt{iz}\right)}{\sqrt{iz}}\right]\right\},$$
$$\frac{\pi n^2 F^2 DaC^\infty}{2RT}\,\Im(Z) = \Im\left\{\frac{1}{\sqrt{iz}}\left[1+\frac{\mathbf{M}_1\left(2\sqrt{iz}\right)}{\sqrt{iz}}\right]\right\},$$

and

$$\Re(Z) = \frac{RT}{\pi nFi_0a^2} + \frac{2RT}{\pi n^2F^2DaC^\infty}\cdot\Phi_{4,A}\left(z\right),$$
$$\Im(Z) = \frac{2RT}{\pi n^2F^2DaC^\infty}\cdot\Phi_{5,A}\left(z\right).$$

The low-frequency limits of each

$$\lim_{z\to 0}\Phi_{4,A}(z) = \frac{8}{3\pi}, \qquad \lim_{z\to 0}\Phi_{5,A}(z) = -\lim_{z\to 0}\frac{\sqrt{z}}{2\sqrt{2}} = 0,$$

provide finite values for a circular disk electrode, as required by Kramers-Kronig theory [7].

A useful asymptotic representation for $\mathbf{M}_1\left(z\right)$ is [18, p. 293, Eq. 11.6.2]

$$\mathbf{M}_\nu\left(z\right) \sim \frac{1}{\pi}\sum_{k=1}^{\infty}\frac{(-1)^{k+1}\,\Gamma\left(k+1/2\right)}{\Gamma\left(\nu+1/2-k\right)\;\;(z/2)^{2k-\nu+1}}, \qquad |\arg(z)| < \tfrac{1}{2}\pi - \delta,$$

from which the high-frequency limits are derived as:

$$\lim_{z\to\infty}\Phi_{4,A}(z) = \lim_{z\to\infty}\frac{1}{\sqrt{2z}} = 0, \qquad \lim_{z\to\infty}\Phi_{5,A}(z) = -\lim_{z\to\infty}\frac{1}{\sqrt{2z}} = 0.$$

Both high- and low-frequency limits are consistent with those obtained by Navarro-Laboulais et al. [7] after scaling by the factor $2/\sqrt{z}$, which equates the new analytic coefficients $\Phi_{4,A}, \Phi_{5,A}$ with the previous integral forms Φ_4, Φ_5 [1]. The maximum value of the imaginary impedance, as shown in Figure 2, evaluates to $\Phi_{5,A} = -0.197294$ at the dimensionless frequency $z = 2.44024$. A value for the dimensionless frequency of 2.4410 has been reported, using a robust anisotropic mesh finite element simulation technique [8], and results from other work include values of 2.5 [9], and 2.5119 [7].

4 Values, accuracy, and precision

The concentration function, $\langle C \rangle$, is readily evaluated using any software package that handles complex-argument Struve and Bessel functions, as well as non-normalized Fresnel integrals. In this work, we used Python 3.14 with the NumPy and SciPy modules for all array operations, modified Bessel functions, and Fresnel integrals. SciPy does not provide complex-argument support for Struve functions, so the modified Struve function, $\mathbf{L}_1(z)$, was evaluated using the mpmath library at 50-digit precision for validation.

After generation, the values determined herein for $\Phi_{4,A}, \Phi_{5,A}$, (direct functions of $\langle C \rangle_1$), were compared to a table of numeric values of integral representations [14] after scaling by 2; see Section 3.

It should be noted that the numerical simulation of the solution to the system described by Equations (3)–(6) has been previously investigated using a number of finite element methods (FEMs) and various adaptations thereof, which were referenced in the introduction. In general, it is difficult to adjust conventional mesh/node numbers in the FEM to simulate phase angles and amplitudes to relative standard errors better than 2%. The problem has special difficulties because with most mesh refinement FEMs, there is a convergence to an asymptotic error floor, consistent with the known sub-optimal convergence rate of linear finite elements at the $1/\sqrt{a^2 - r^2}$ concentration gradient singularity at the electrode edge at $r = a$. The problem seems true when dealing with many power-series-based functions.

Recently, these problems have been successfully treated by more advanced techniques, especially in the important work by Michel et al. [8]. That work describes the use of anisotropic mesh adaptation to attain significantly lower errors. The work described therein presents accurate simulations of the same differential equation system that we have solved analytically in this work, *i.e.*, both components $\langle C \rangle_1 + \langle C \rangle_2$ are included in the simulation. We compare the analytic values here with parts of the Michel et al.'s numerical simulations, as well as with other values reported in the literature.

A value of significance to check is the value of the dimensionless frequency at which the imaginary component of the diffusion impedance is a maximum when plotting the Nyquist negative imaginary component vs. the real component of the diffusion impedance, i.e., Figure 2. The values of the two components $\Phi_{4,A}, \Phi_{5,A}$ are calculated according to the standard procedure given in Section 3, using the calculated values of $\langle C \rangle$. The plot, which manifests the solution of $\langle C \rangle$ over all frequencies, shows that the maximum value is at dimensionless frequency $z = 2.44024$. Michel et al. report a simulated value of $z = 2.4410$, a relative error of approximately 0.00033. Also to be compared to the value of $z = 2.44024$ are those values from other work, e.g., 2.5 [9], and 2.5119 [7].

The analytic value of the maximum negative imaginary impedance component at that frequency is found to be 0.394588, and Michel et al. report 0.3950, a relative error of 0.0010.

5 Stability analysis

As the particular diffusion equation system in Subsection 2.1 has not previously been fully resolved analytically, comments on its boundedness for all times and decay of any initial perturbations and/or transients are in order. However, at the outset, it is also fair to say that the system is a diffusive one, and the Laplacian is negative-definite. It belongs, therefore, to one of the few classes of partial differential equations that are provably stable for all (real and positive) values of its parameters. Here are some general comments to support this:

To consider first the decay of boundary conditions, the source-free (homogeneous) diffusion equation with homogeneous boundary conditions reads

$$\frac{1}{D}\frac{\partial\langle C\rangle}{\partial t} = \nabla^2\langle C\rangle, \qquad \left.\frac{\partial\langle C\rangle}{\partial z}\right|_{z=0} = 0, \quad \langle C\rangle \to 0 \text{ as } r, z \to \infty.$$

This system, solved by the method of separation of variables using a Fourier transform for the z coordinate and a Hankel transform for the r coordinate, yields spatial eigenfunctions of the differential operator $D\nabla^2$ that comprise eigenvalues $\lambda \leq 0$; the accompanying time dependency follows as $e^{\lambda t}$. Since λ is strictly negative for all non-trivial modes, each homogeneous solution will decay exponentially to zero as $t \to \infty$. As the original problem specifies a zero condition at $z \to \infty$, the first (zero) eigenvalue is excluded, so indeed, the homogeneous problem is asymptotically (indeed, exponentially) stable.

Next is the question of boundedness stability of input vs. output. Note that defined imposed input flux is

$$D\left.\frac{\partial\langle C\rangle}{\partial z}\right|_{z=0} = -Q\sin(\omega t), \quad (0 \leq r < a), \qquad 0 \text{ otherwise.}$$

This is a linear system driven by a bounded, periodic input. As seen in Section 2, the full solution $\langle C\rangle$ can be written as the sum of a transient homogeneous solution (which decays) and a particular solution that inherits the time-dependence of the sinusoidal perturbation. Since the spatial operator therein is self-adjoint and negative semi-definite on the appropriate Hilbert space (with the given boundary conditions), it generates a contraction semigroup. Standard semigroup theory guarantees that for any bounded, continuous forcing, the solution exists globally, remains bounded, and depends continuously on the initial data and the boundary input. In physical terms, the periodic sinusoidal flux adds and removes mass; the concentration field $\langle C\rangle$ oscillates at the driving frequency ω without unbounded growth: thermodynamically, pure diffusion is strongly dissipative, preventing formation of any resonance or parametric instability.

Considering next the long-time periodic state (or frequency domain) analysis, to verify its boundedness, it can be summarized from Appendix 7, by looking for an arbitrary time-periodic steady-state solution like

$$\langle C\rangle(r, z, t) = \mathrm{Im}\big[\langle\hat{C}\rangle(r, z, \omega)\, e^{i\omega t}\big].$$

Substituting yields the following modified Helmholtz equation:

$$i\frac{\omega}{D}\langle\hat{C}\rangle = \frac{\partial^2\langle\hat{C}\rangle}{\partial r^2} + \frac{1}{r}\frac{\partial\langle\hat{C}\rangle}{\partial r} + \frac{\partial^2\langle\hat{C}\rangle}{\partial z^2},$$

with boundary condition $D\,\partial_z\langle\hat{C}\rangle|_{z=0} = -Q$ for $r < a$ and 0 otherwise. Applying the Hankel transform of order zero in r and solving a simple second-order ODE in z gives

$$\langle\hat{C}\rangle \propto \int_0^\infty \frac{J_0(kr)\, J_1(ka)}{k\sqrt{k^2 + i\omega/D}}\, e^{-z\sqrt{k^2+i\omega/D}}\, dk,$$

which is well-defined and bounded for all $\omega > 0$ because $\Re\sqrt{k^2 + i\omega/D} > 0$. The amplitude of the concentration oscillation is finite everywhere and decays to zero as $r, z \to \infty$, confirming the stability of the transition of the "bounded input" to the "bounded output".

Finally, consider the issue of the Hadamard concept of "well-posedness" of an equation. It is specified that there is a unique solution at all times $t \geq 0$, and the solution depends continuously on the initial condition and the defined boundary flux. One such set of properties follows from the maximum principle and energy estimates, e.g., multiply the partial differential equation by $\langle C\rangle$ and integrate over the entire half-space above the disk electrode, giving

$$\frac{1}{2D}\frac{d}{dt}\|\langle C\rangle\|^2 + \|\nabla\langle C\rangle\|^2 = -\int_{z=0} (\partial_z\langle C\rangle)\langle C\rangle\, dA = \text{boundary work},$$

which dissipates energy unless driven. (Here, $\|\nabla\langle C\rangle\|$ represents the L^2 norm of the entire averaged concentration field.) The system is unconditionally stable.

6 Electrochemical parameter sensitivity and temporal response

This section presents a parametric analysis for the behavior of the average concentration $\langle C\rangle$ for a disk electrode under a sinusoidal flux $Q\sin(\omega t)$. The system itself is governed by Fick's second law of diffusion and is unconditionally stable for all physically meaningful parameters ($D > 0$, $a > 0$, $\omega > 0$). The analysis then focuses on quantifying the system's response characteristics and sensitivity to variations in those parameters. In order to provide wide ranges of parameter analysis, it is convenient to fix, as applicable in each of the plots, values for other parameters at sensible values. Here, these are taken to be those for a typical microelectrode, and typical aqueous/non-aqueous diffusion coefficients. For simple scaling, a nominal unit flux is assumed; i.e., $Q = 1$ mol/(cm^2 s), $D = 10^{-5}$ cm^2/s, $a = 0.01$ cm, $\omega = 1$ rad/s (as applicable).

Figure 3 shows the transient region from initial equilibrium at the application of flux to attainment of the periodic steady-state. There is an initial transient of amplitude $\propto \sqrt{t}$. Two characteristic timescales govern the transient decay: $1/\omega$ (the period of an oscillation), and a^2/D (a characteristic time representing diffusion time across the disk). After $t \gtrsim \max(1/\omega, a^2/D)$, the transient $\langle C\rangle_2$ portion has decayed to zero, and the system has reached a purely sinusoidal steady-periodic state; this clearly implies the entire system is asymptotically stable with timescale the larger of either the electrochemical (ω^{-1}) or the diffusion (a^2/D) timescales.

The amplitude of $\langle C\rangle$ is displayed in Figure 4 as a function of the experimental angular frequency. Once again, three distinct regions are visible, in this case measured over a wide range of frequencies used in typical electrochemical experiments. At low frequencies, $\omega \ll D/a^2$, $\beta \ll 1$, the amplitude scales as $1/\omega$; the diffusion layer extends far beyond the disk, and the system behaves like a point source. When the frequency approaches $\omega \sim D/a^2$, $\beta \sim 1$, there is a transition where the diffusion layer thickness $\delta = \sqrt{2D/\omega}$ starts to be comparable to the disk radius a. This is a region of maximum sensitivity to frequency change. Continued increase in applied frequency $\omega \gg D/a^2$, $\beta \gg 1$ scales the amplitude as $1/\sqrt{\omega}$; the diffusion layer is now very thin, and the electrode surface appears electrochemically as an infinite plane. Figure 5 displays the amplitude calculated as a function of the system's general dimensionless parameter β. All parameter combinations collapse onto a single master curve when plotted against β. $\beta = 1$ is the "critical" value that separates the two regions: (1) The "point-source" region ($\beta \ll 1$) in which the disk is small relative to the diffusion layer, the diffusion processes at the edge of the disk dominate the total flux. (2) The infinite-plane regime ($\beta \gg 1$) where diffusion of the "large" surface area of the disk relative to the diffusion layer reduces the effects seen at

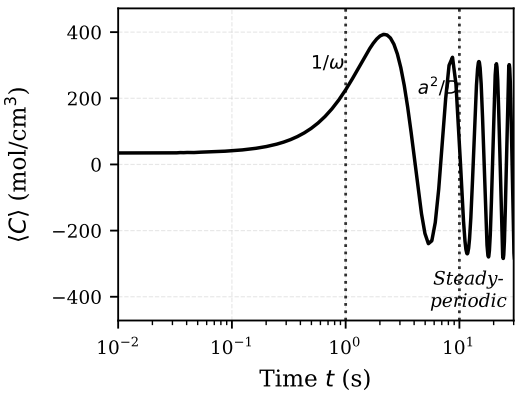


Figure 3: Time evolution of $\langle C \rangle$ showing transient decay to steady-periodic behavior.

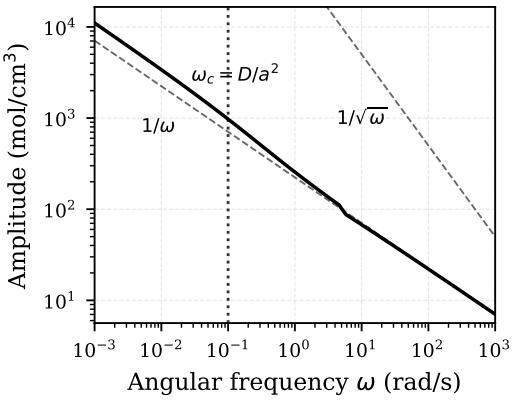


Figure 4: Amplitude of $\langle C \rangle$ as a function of angular frequency ω.

the edge; edge effects become negligible. The transition between the two regions is smooth but rapid in the region $0.1 < \beta < 10$. Choosing β values judiciously allows scaling results between different electrode sizes, diffusion coefficients, and frequencies without repeating experiments or simulations.

In Figure 6, the amplitude of $\langle C \rangle$ is shown this time as sensitivity to the diffusion coefficient D. Two scaling regions are defined. At small D, ($D \ll \omega a^2$, $\beta \gg 1$), the amplitude scales as $D^{-1/2}$. Slower diffusion leads to higher concentration buildup close to the surface. At large values of D ($D \gg \omega a^2$, $\beta \ll 1$), the amplitude scales as D^{-1}. Faster diffusion spreads the concentration over a larger volume. The maximum sensitivity to D occurs at $D_c = \omega a^2$, where $\beta = 1$. Typically, the value of the diffusion coefficient is the most critical parameter for quantitative measurements. Small errors in D cause large errors in concentration near D_c. For applications requiring high accuracy/precision measurements, one chooses to operate in the parameter region sensitivity is lower, e.g., very high or very low D. Figure 7 provides the

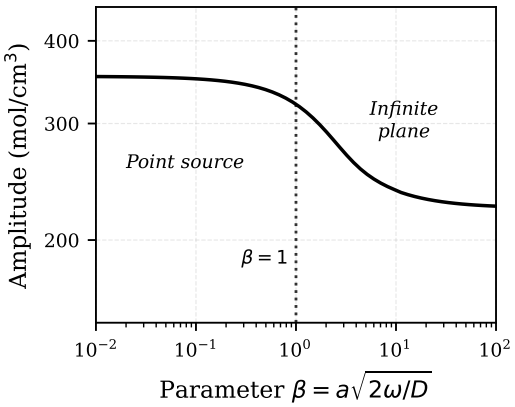


Figure 5: Sensitivity to the dimensionless parameter $\beta = a\sqrt{2\omega/D}$.

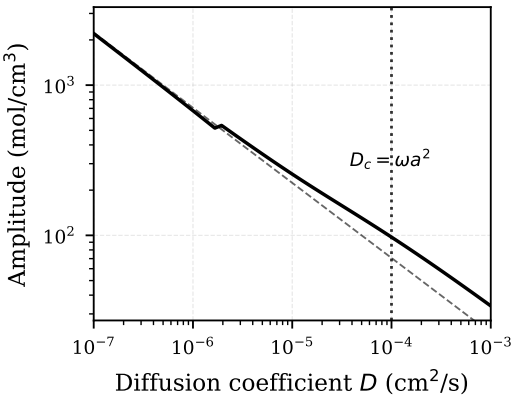


Figure 6: Sensitivity to the diffusion coefficient D.

sensitivity plot for the amplitude of the surface concentration for the last parameter a, the

circular disk electrode radius. For small disks $a \ll \sqrt{D/\omega}$, $\beta \ll 1$, the observed amplitude is nearly independent of a, and the disk acts as a point source. At large disks ($a \gg \sqrt{D/\omega}$, $\beta \gg 1$), the amplitude saturates; the disk acts as an infinite plane. The transition between these occurs at $a_c = \sqrt{D/\omega}$, where $\beta = 1$, *i.e.*, where the disk radius equals the diffusion layer thickness. Hence, for optimal sensitivity to radius variations, choose $a \sim a_c$. For applications requiring radius-independent measurements, use very small disks ($a \ll \delta$).

Figure 8 is a two-parameter plot depicting the amplitude of the concentration as a function of both the diffusion coefficient D and the frequency ω. The $\beta = 1$ line (white dashed) separates the point-source ($\beta < 1$) and infinite-plane ($\beta > 1$) regions discussed above. The amplitude is highest for small D and small ω (lower-left region) and lowest for large D and large ω (upper-right region). The transition is sharpest for intermediate values where D and ω are balanced.

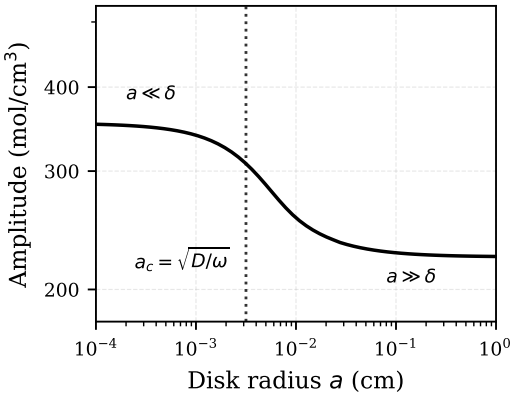


Figure 7: Sensitivity to the circular disk radius a.

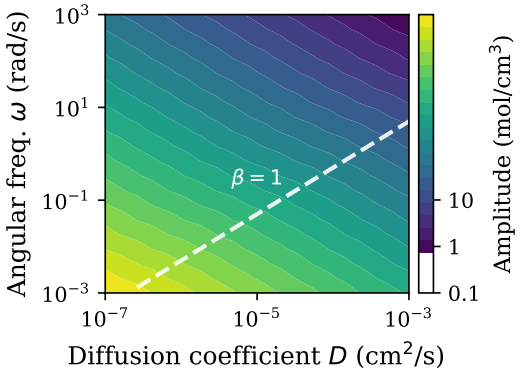


Figure 8: Two-parameter sensitivity map showing the amplitude as a function of D and ω.

7 Conclusion

This paper presents a total solution for the time-dependent average surface concentration of a diffusing electroactive species at a circular disk electrode subjected to a periodic flux perturbation. The solution comprises two distinct contributions: one for the transient response to the perturbation and the other for the eventual steady periodic state, expressed in terms of a modified Struve function.

The analytic form of the real and imaginary components to the electrochemical diffusion impedance is also found in the form of a modified Struve function from the steady-state contribution to the concentration.

The described mathematical system is found to be unconditionally stable, both asymptotically and exponentially. A sensitivity analysis of the concentration profile to its parameters is presented. The behavior is governed by the dimensionless parameter $\beta = a\sqrt{2\omega/D}$, enabling a convenient and comprehensive parameter sensitivity analysis.

Regarding further work in this area, the use of the full expression in AC voltammetric methods is to be explored in detail. Also in mind is the application of the transient part of

the solution in potential steps with superimposed AC, as well as AC relaxation. In impedance measurements, incorporating automatic control of time-of-measurement vs. frequency to allow for full decay transient effects is of use.

In addition, the transient concentration profiles themselves are of significant interest in real-time spectroelectrochemical studies at and near electrode surfaces. In such studies, temporal visible and infrared spectra of reactants, intermediates, and products can determine reaction pathways and kinetics. There is already a significant advantage in using AC-based electrochemical measurement techniques, as they can be combined with phase-sensitive detection and fast Fourier transform techniques. The results presented herein must be incorporated into the necessary expressions for optical absorbance-time response equations applied to specific spectroelectrochemical experiments. The goal is to enable the capability to monitor the transient concentrations of individual reactants and products.

Appendix

The Laplace transform for the general solution of the concentration measure $\bar{C}$ in the system Equations (3)-(6) is [1]

$$\bar{C} = \frac{Q\omega a}{D(s^2+\omega^2)} \int_0^\infty \exp\left(-\left(\alpha^2+q^2\right)z\right) J_0(\alpha r)\, J_1(\alpha a)\, \frac{\mathrm{d}\alpha}{(\alpha^2+q^2)^{1/2}}, \tag{17}$$

with $q^2 = s/D$, and Bessel functions of the first kind $J_0(z)$ and $J_1(z)$ of the orders 0 and 1, respectively. Using two Bessel identities [19]

$$\int_\delta^{\delta+2\pi} J_0(\alpha R)\, d\,\psi' = 2\pi J_0(\alpha\rho), \omega \in \mathbb{R}, \qquad \int_0^a \rho' J_0(\alpha\rho')\, d\,\rho' = \frac{a}{\alpha} J_1(\alpha a),$$

the result, after normalizing to the area of the disk, shows that the Laplace transformed average concentration over the surface ($0 \leqslant r < a, z = 0$) is

$$\langle\bar{C}\rangle = \frac{2Q\omega}{D(s^2+\omega^2)} \int_0^\infty \frac{J_1^2(\sigma a)}{\sigma} \frac{\mathrm{d}\sigma}{(\sigma^2+q^2)^{1/2}}, \quad q^2 = \frac{s}{D}. \tag{18}$$

Now consider the integral function of parameter a

$$I(a) = \int_0^\infty \frac{J_1^2(\sigma a)}{\sigma} \frac{\mathrm{d}\sigma}{\sqrt{\sigma^2+b^2}}.$$

Application of a pair of identities sourced from the properties of Bessel functions [20, see contribution by H. Levine therein] [21], i.e.,

$$\left(\frac{\mathrm{d}^2}{\mathrm{d}^2 a} + \frac{3}{a}\frac{\mathrm{d}}{\mathrm{d}a}\right) I(a) = 2J_0^2(a) - 2J_1^2(a) = \frac{4}{\pi}\int_0^\pi \sin\mu^2\, J_0(2a\sin\mu)\,\mathrm{d}\mu,$$

to $I(a)$ provides that

$$\left(\frac{\mathrm{d}^2}{\mathrm{d}^2 a} + \frac{3}{a}\frac{\mathrm{d}}{\mathrm{d}a}\right) I(a) = \frac{4}{\pi}\int_0^\pi \sin^2\psi\ \mathrm{d}\psi \int_0^\infty J_0(2\sigma a\sin\psi)\frac{\sigma\mathrm{d}\sigma}{\sqrt{\sigma^2+b^2}}$$

$$= \frac{4}{\pi}\int_0^{\pi} \sin^2\psi \frac{\exp\left(-2ab\sin\psi\right)}{2a\sin\psi}\,\mathrm{d}\psi = \frac{2}{\pi a}\int_0^{\pi} \sin\psi\ \mathrm{e}^{-2ab\sin\psi}\mathrm{d}\psi,$$

and with $\lambda = 2ab$, the last integral reduces to

$$\int_0^{\pi} \sin\psi\ \mathrm{e}^{-\lambda\sin\psi}\mathrm{d}\psi = \frac{\mathrm{d}}{\mathrm{d}\lambda}\int_0^{\pi} \mathrm{e}^{-\lambda\sin\psi}\mathrm{d}\psi,$$

in which

$$\int_0^{\pi} \mathrm{e}^{-\lambda\sin\psi}\mathrm{d}\psi = 2\int_0^{\pi/2} \mathrm{e}^{-\lambda\sin\psi}\mathrm{d}\psi = 2\int_0^{\pi/2} \mathrm{e}^{-\lambda\cos\eta}\mathrm{d}\eta = \pi\left[I_0\left(\lambda\right) - \mathbf{L}_0\left(\lambda\right)\right],$$

whence

$$\int_0^{\pi} \sin\psi\ \mathrm{e}^{-\lambda\sin\psi}\mathrm{d}\psi = \pi\left[\frac{2}{\pi} + I_0\left(\lambda\right) - \mathbf{L}_0\left(\lambda\right)\right].$$

Now, noting that [18, p. 288]

$$\mathbf{L}_\nu(x) = \sum_{n=0}^{\infty} \frac{\left(\frac{z}{2}\right)^{2n+\nu+1}}{\Gamma(n+3/2)\Gamma(n+\nu+3/2)}, \qquad I_\nu(x) = \sum_{n=0}^{\infty} \frac{\left(\frac{z}{2}\right)^{2n+\nu}}{n!\,\Gamma(n+\nu+1)},$$

where, in these functions, the cases $\nu = 0, 1$, used in the sequel, result in:

$$\mathbf{L}_0(x) = \frac{2x}{\pi} + \frac{2x^3}{9\pi} + \cdots, \qquad \mathbf{L}_1(x) = \frac{2x^2}{3\pi} + \frac{2x^4}{45\pi} + \cdots, \tag{19}$$

$$I_0(x) = 1 + \frac{x^2}{4} + \cdots, \qquad I_1(x) = \frac{x}{2} + \frac{x^3}{16} + \cdots, \tag{20}$$

and the modified Struve function of the second kind of the order ν is defined by $\mathbf{M}_1(x)$ [18, p. 288, Eq. 11.2.6]

$$\mathbf{M}_\nu(x) = \mathbf{L}_\nu(x) - I_\nu(x).$$

Returning to the differentiation of $I(a)$,

$$\frac{1}{a^3}\frac{\mathrm{d}}{\mathrm{d}a}\left(a^3\frac{\mathrm{d}I}{\mathrm{d}a}\right) = \frac{2}{a}\left[\frac{2}{\pi} + \mathbf{L}_1\left(2ab\right) - I_1\left(2ab\right)\right],$$

$$\frac{\mathrm{d}}{\mathrm{d}a}\left(a^3\frac{\mathrm{d}I}{\mathrm{d}a}\right) = 2a^2\left[\frac{2}{\pi} + \mathbf{L}_1\left(2ab\right) - I_1\left(2ab\right)\right],$$

$$a^3\frac{\mathrm{d}I}{\mathrm{d}a} = \frac{4a^3}{3\pi} + 2\int_0^{a}\left[\pi^2\mathbf{L}_1(2bx) - I_1(2bx)x^2\right]\mathrm{d}x,$$

wherein reduction of the two integrals

$$\int_0^{a} x^2 I_1\left(\mu x\right)\mathrm{d}x = \frac{1}{\mu}\int_0^{a} x^2\mathrm{d}I_0\left(\mu x\right)\mathrm{d}x = \frac{a^2}{\mu}I_0(\mu a) - \frac{2}{\mu}\int_0^{a} xI_0\left(\mu x\right)\mathrm{d}x$$

$$= \frac{a^2}{\mu} I_0(\mu a) - \frac{2a}{\mu^2} I_1(\mu a)\,,$$

and

$$\int_0^a x^2 \mathbf{L}_1(\mu x)\mathrm{d}x = \int_0^a x^2 \left[\frac{1}{\mu}\frac{\mathrm{d}}{\mathrm{d}x}\mathbf{L}_0(\mu x) - \frac{2}{\pi}\right]\mathrm{d}x$$

$$= -\frac{2a^3}{3\pi} + \frac{a^2}{\mu}\mathbf{L}_0(\mu a) - \frac{2}{\mu}\int_0^a x\mathbf{L}_0(\mu x)\mathrm{d}x = -\frac{2a^3}{3\pi} + \frac{a^2}{\mu}\mathbf{L}_0(\mu a) - \frac{2a}{\mu^2}\mathbf{L}_1(\mu a),$$

provide the differential equation

$$\begin{aligned} a^3\frac{dI}{da} &= \frac{4a^3}{3\pi} + 2\left\{-\frac{2a^2}{3\pi} + \frac{a^2}{2b}\mathbf{L}_0\left(2ab\right) - \frac{2a}{4b^2}\mathbf{L}_1(2a)\right\} \\ &\qquad - 2\left\{\frac{a^2}{2b}I_0(2ab) - \frac{2a}{4b^2}I_1(2ab)\right\} \\ &= \frac{a^2}{b}\mathbf{L}_0(2ab) - \frac{a}{b^2}\mathbf{L}_1(2ab) - \frac{a^2}{b}I_0(2ab) + \frac{a}{b^2}I_1(2ab), \\ \therefore \frac{dI}{da} &= \frac{1}{ab}\mathbf{L}_0(2ab) - \frac{1}{a^2b^2}\mathbf{L}_1(2ab) - \frac{1}{ab}I_0(2ab) + \frac{1}{a^2b^2}I_1(2ab), \end{aligned}$$

which integrates to

$$I = \frac{1}{b}\int_0^a \frac{1}{x}\mathbf{L}_0(2bx)\mathrm{d}x - \frac{1}{b^2}\int_0^a \frac{1}{x^2}\mathbf{L}_1(2bx)\mathrm{d}x - \int_0^a \left\{\frac{1}{bx}I_0(2bx) - \frac{1}{b^2x^2}I_1\left(2bx\right)\right\}\mathrm{d}x. \tag{21}$$

The third integral therein

$$\int_0^a \left\{\frac{1}{b^2x^2}I_1(2bx) - \frac{1}{bx}I_0(2bx)\right\}\mathrm{d}x = \frac{2}{b}\int_0^{2ab}\frac{1}{y^2}\left[I_1(y) - \frac{1}{2y^{-1}}I_0(y)\right]\mathrm{d}y,$$

may be reduced by considering

$$F_1(\lambda) = \int_0^\lambda \frac{1}{y^2}\left[I_1(y) - \frac{1}{2y^{-1}}I_0(y)\right]\mathrm{d}y = \int_0^\lambda \mathrm{d}(-y^{-1})\left[I_1\left(y\right) - \frac{y}{2}I_0(y)\right]\mathrm{d}y$$

$$= -\frac{1}{\lambda}\left[I_1(\lambda) - \frac{\lambda}{2}I_0(\lambda)\right] + \int_0^\lambda \frac{1}{y}\left[I_0(y) - \frac{I_0(y)}{y} - \frac{1}{2}I_0(y) - \frac{y}{2}I_1(y)\right]\mathrm{d}y,$$

$$2F_1(\lambda) = -\frac{1}{\lambda}I_1(\lambda) + \frac{1}{2}I_0(\lambda) - \frac{1}{2}\left[I_0\left(\lambda\right) - 1\right] = \frac{1}{2} - \frac{1}{\lambda}I_1(\lambda),$$

$$\therefore F_1(\lambda) = \frac{1}{4} - \frac{1}{2\lambda}I_1(\lambda). \tag{22}$$

Upon checking same by differentiation:

$$\frac{\mathrm{d}}{\mathrm{d}\lambda}\int_0^\lambda \frac{1}{y^2}\left[I_1(y) - \frac{y}{2}I_0(y)\right]\mathrm{d}y = \frac{1}{\lambda^2}I_1(\lambda) - \frac{1}{2\lambda}I_0(\lambda) = \frac{\mathrm{d}}{\mathrm{d}\lambda}\left[-\frac{1}{2\lambda}I_1(\lambda)\right]$$

$$= \frac{1}{2\lambda^2} I_1(\lambda) - \frac{1}{2\lambda}\left[I_0(\lambda) - \frac{I_0(\lambda)}{\lambda}\right] = \frac{1}{\lambda^2} I_1(\lambda) - \frac{1}{2\lambda} I_0(\lambda),$$

which is consistent with the first line of Equation (22). Return to the first two integrals in Equation (21) and rearrange to

$$\int_0^a \left[\frac{1}{b^2x^2}\mathbf{L}_1(2bx) - \frac{1}{bx}\mathbf{L}_0(2bx)\right] \mathrm{d}x = \frac{2}{b}\int_0^{2ab} \frac{1}{y^2}\left[\mathbf{L}_1(y) - \frac{y}{2}\mathbf{L}_0(y)\right] \mathrm{d}y,$$

and consider again by partial integration

$$\begin{aligned} F_2(\lambda) &= \int_0^\lambda \frac{1}{y^2}\left[\mathbf{L}_1(y) - \frac{y}{2}\mathbf{L}_0(y)\right] \mathrm{d}y = \int_0^\lambda \mathrm{d}(-y^{-1})\left[\mathbf{L}_1(y) - \frac{y}{2}\mathbf{L}_0(y)\right] \mathrm{d}y \\ &= -\frac{1}{\lambda}\left[\mathbf{L}_1(\lambda) - \frac{\lambda}{2}\mathbf{L}_0(\lambda)\right] \\ &\quad + \int_0^\lambda \frac{1}{y}\left[\mathbf{L}_0(y) - \frac{\mathbf{L}_1(y)}{y} - \frac{1}{2}\mathbf{L}_0(y) - \frac{y}{2}\left\{\mathbf{L}_1(y) + \frac{2}{\pi}\right\}\right] \mathrm{d}y, \end{aligned} \tag{23}$$

$$\begin{aligned} 2F_2(\lambda) &= -\frac{1}{\lambda}\mathbf{L}_1(\lambda) + \frac{1}{2}\mathbf{L}_0(\lambda) - \frac{\lambda}{\pi} - \frac{1}{2}\int_0^\lambda \mathbf{L}_1(y)\mathrm{d}y = -\frac{1}{\lambda}\mathbf{L}_1(\lambda) + \frac{1}{2}\mathbf{L}_0(\lambda) \\ &\quad - \frac{\lambda}{\pi} - \frac{1}{2}\left[\mathbf{L}_0(\lambda) - \frac{2\lambda}{\pi}\right] = -\frac{1}{\lambda}\mathbf{L}_1(\lambda), \\ \therefore\ F_2(\lambda) &= -\frac{1}{2\lambda}\,\mathbf{L}_1(\lambda). \end{aligned} \tag{24}$$

Checking this result by differentiation

$$\frac{\mathrm{d}F_2(\lambda)}{\mathrm{d}\lambda} = \frac{1}{2\lambda^2}\mathbf{L}_1(\lambda) - \frac{1}{2\lambda}\left[\mathbf{L}_0(\lambda) - \frac{\mathbf{L}_1(\lambda)}{\lambda}\right], = \frac{1}{\lambda^2}\mathbf{L}_1(\lambda) - \frac{1}{2\lambda}\mathbf{L}_0(\lambda),$$

confirms the original integral in Equation (23). Assembling the two components $F_1(\lambda), F_2(\lambda)$,

$$\begin{aligned} I(a) &= \int_0^\infty \frac{J_1^2(\sigma a)}{\sigma}\frac{\mathrm{d}\sigma}{\sqrt{\sigma^2+b^2}} = \frac{1}{2b} - \frac{1}{2ab^2}\left[I_1(2ab) - \mathbf{L}_1(2ab)\right] \\ &= \frac{1}{b} + \frac{1}{2ab^2}\,\mathbf{M}_1(2ab). \end{aligned}$$

and Equation (18) becomes

$$\langle \bar{C} \rangle = \frac{2Q\omega}{D(s^2+\omega^2)}\left\{\frac{1}{2q} - \frac{2}{\pi q}\int_0^{\pi/2} \sin^2\varphi \mathrm{e}^{-2aq\cos\varphi}\mathrm{d}\varphi\right\} = \frac{2Q\omega}{D(s^2+\omega^2)}\left\{\frac{1}{2q} + \frac{\mathbf{M}_1\left(2aq\right)}{2aq^2}\right\}. \tag{25}$$

Note then that an appropriate variable change therein provides the convenient and asymptotically equivalent representation (based on Equations (19) and (20)):

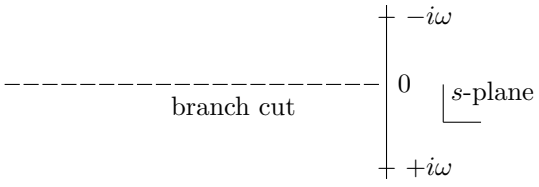
$$I = \int_0^\infty \frac{J_1^2(ab\lambda)}{\lambda}\frac{\mathrm{d}\lambda}{\sqrt{\lambda^2+1}} = \frac{1}{2} - \frac{1}{2ab}\left[I_1(2ab) - \mathbf{L}_1(2ab)\right]$$

$$\sim \frac{1}{2} - \frac{1}{2ab}\left(\frac{1}{2}(2ab) - \frac{2}{3\pi}(2ab)^2 \cdots\right) \to \frac{4}{3\pi}ab, \qquad ab \to 0\,.$$

This expression readily shows that the dimensionless flux $Dc^{\infty}/2Qa$ at a disk electrode is limited at high values of dimensionless time $b = \sqrt{Dt/a^2}$ to values $\leq 4/3\pi$ at disk electrodes of radius a under constant or linear swept amperometric conditions [22].

Inversion to the time domain of Equation (25) to $\langle C\rangle$ comprises the evaluation of the Bromwich form

$$\langle C\rangle = \mathcal{L}^{-1}\left(\langle\bar{C}\rangle\right) = \frac{1}{2\sqrt{D}\,\pi\,i}\int\limits_{\uparrow} \mathrm{e}^{st}\frac{Q\omega}{\sqrt{p}\,(p^2+\omega^2)}\cdot\left\{1 - \frac{4}{\pi}\int\limits_0^{\pi/2}\sin^2\varphi \mathrm{e}^{-2a\sqrt{s/D}\cos\varphi}\mathrm{d}\varphi\right\}\mathrm{d}p, \quad (26)$$



which contains the separate steady-periodic contribution due to the poles at $s = \pm i\omega$, as well as the temporal diffusional contribution from the branch cut along the negative real axis of the s-plane. Denoting the respective contributions by $\langle C\rangle_1, \langle C\rangle_2$, the first (steady periodic state) is expressed by

$$\begin{aligned}
\langle C\rangle_1 = {} & \frac{1}{2\pi\,i}\cdot 2\pi i\,\mathrm{e}^{i\omega t}\frac{2Q\omega}{2i\omega D}\left\{\frac{\mathrm{e}^{-i\pi/4}}{2\sqrt{\omega/D}}\right. \\
& \left. -\frac{2\mathrm{e}^{-i\pi/4}}{\pi\sqrt{\omega/D}}\int\limits_0^{\pi/2}\sin^2\varphi\,\exp\left(-2a\sqrt{\frac{\omega}{D}}\frac{1+i}{\sqrt{2}}\cos\varphi\right)\mathrm{d}\varphi\right\} \\
& + \frac{1}{2\pi\,i}\cdot 2\pi i\,\mathrm{e}^{i\omega t}\frac{2Q\omega}{-2i\omega D}\left\{\frac{\mathrm{e}^{i\pi/4}}{2\sqrt{\omega/D}}\right. \\
& \left. -\frac{2\mathrm{e}^{i\pi/4}}{\pi\sqrt{\omega/D}}\int\limits_0^{\pi/2}\sin^2\varphi\,\exp\left(-2a\sqrt{\frac{\omega}{D}}\frac{1-i}{\sqrt{2}}\cos\varphi\right)\mathrm{d}\varphi\right\} \\
= {} & \frac{Q}{\sqrt{D\omega}}\,\Re\left\{-\frac{1+i}{\sqrt{2}}\mathrm{e}^{i\omega t}\left[1\right.\right. \\
& \left.\left. -\frac{4}{\pi}\int\limits_0^{\pi/2}\sin^2\varphi\exp\left(-a\sqrt{\frac{2\omega}{D}}\cos\varphi\right)\exp\left(-ia\sqrt{\frac{2\omega}{D}}\cos\varphi\right)\mathrm{d}\varphi\right]\right\},
\end{aligned}$$

and the transient bulk diffusion component by

$$\begin{aligned}
\langle C\rangle_2 &= \frac{1}{2\pi i}\int_{\infty}^{0}\frac{\mathrm{e}^{-\sigma t}(-\mathrm{d}\sigma)}{\sigma^2+\omega^2}\cdot\frac{2Q\omega}{D}\left\{\frac{\mathrm{e}^{i\pi/2}}{2\sqrt{\sigma/D}}\right.\\
&\qquad\left.-\frac{2\mathrm{e}^{i\pi/2}}{\pi\sqrt{\sigma/D}}\int_0^{\pi/2}\sin^2\varphi\exp\left(2ia\sqrt{\frac{\sigma}{D}}\cos\varphi\right)\mathrm{d}\varphi\right\}\\
&\quad+\frac{1}{2\pi i}\int_{0}^{\infty}\frac{\mathrm{e}^{-\sigma t}(-\mathrm{d}\sigma)}{\sigma^2+\omega^2}\cdot\frac{2Q\omega}{D}\left\{\frac{\mathrm{e}^{-i\pi/2}}{2\sqrt{\sigma/D}}\right.\\
&\qquad\left.-\frac{2\mathrm{e}^{-i\pi/2}}{\pi\sqrt{\sigma/D}}\int_0^{\pi/2}\sin^2\varphi\exp\left(-2ia\sqrt{\frac{\sigma}{D}}\cos\varphi\right)\mathrm{d}\varphi\right\}\\
&=\frac{Q\omega}{2\pi\sqrt{D}}\int_0^{\infty}\frac{\mathrm{e}^{-\sigma t}\mathrm{d}\sigma}{(\sigma^2+\omega^2)\sqrt{\sigma}}\left\{1-\frac{4}{\pi}\int_0^{\pi/2}\sin^2\varphi\exp\left(-2ia\sqrt{\frac{\sigma}{D}}\cos\varphi\right)\mathrm{d}\varphi\right\}\\
&\quad+\frac{Q\omega}{2\pi\sqrt{D}}\int_0^{\infty}\frac{\mathrm{e}^{-\sigma t}\mathrm{d}\sigma}{(\sigma^2+\omega^2)\sqrt{\sigma}}\left\{1-\frac{4}{\pi}\int_0^{\pi/2}\sin^2\varphi\exp\left(2ia\sqrt{\frac{\sigma}{D}}\cos\varphi\right)\mathrm{d}\varphi\right\}\\
&=\frac{Q\omega}{\pi\sqrt{D}}\int_0^{\infty}\frac{\mathrm{e}^{-\sigma t}\mathrm{d}\sigma}{(\sigma^2+\omega^2)\sqrt{\sigma}}\left\{1-\frac{4}{\pi}\int_0^{\pi/2}\sin^2\varphi\cos\left[2a\sqrt{\frac{\sigma}{D}}\cos\varphi\right]\mathrm{d}\varphi\right\}.
\end{aligned}$$

Checking that $\langle C\rangle_1+\langle C\rangle_2=0$ at $t=0$, note

$$\begin{aligned}
\langle C\rangle_1\Big|_{t=0} &= \frac{Q}{\sqrt{D\omega}}\,\Re\left\{-\frac{1+i}{\sqrt{2}}\left[1\right.\right.\\
&\qquad\left.\left.-\frac{4}{\pi}\int_0^{\pi/2}\sin^2\varphi\cdot\exp\left(-(1+i)a\sqrt{\frac{2\omega}{D}}\cos\varphi\right)\mathrm{d}\varphi\right]\right\}\\
&=-\frac{Q}{\sqrt{2D\omega}}\left\{1-\frac{4}{\pi}\int_0^{\pi/2}\sin^2\varphi\left[\cos\left(a\sqrt{\frac{2\omega}{D}}\cos\varphi\right)\right.\right.\\
&\qquad\left.\left.+\sin\left(a\sqrt{\frac{2\omega}{D}}\cos\varphi\right)\right]\exp\left(-a\sqrt{\frac{2\omega}{D}}\cos\varphi\right)\mathrm{d}\varphi\right\},\\
\langle C\rangle_2\Big|_{t=0} &= \frac{2Q\omega}{\pi\sqrt{D}}\int_0^{\infty}\frac{\mathrm{d}\alpha}{\alpha^4+\omega^2}\left\{1-\frac{4}{\pi}\int_0^{\pi/2}\sin^2\varphi\cos\left[2a\frac{\alpha}{\sqrt{D}}\cos\varphi\right]\mathrm{d}\varphi\right\}
\end{aligned}$$

$$= \frac{Q}{\sqrt{2D\omega}}\left\{1 - \frac{4}{\pi}\int_0^{\pi/2} \sin^2\varphi \left[\cos\left(a\sqrt{\frac{2\omega}{D}}\cos\varphi\right) + \sin\left(a\sqrt{\frac{2\omega}{D}}\cos\varphi\right)\right] \exp\left(-a\sqrt{\frac{2\omega}{D}}\cos\varphi\right)\, \mathrm{d}\varphi\right\},$$

whence $\langle C\rangle_1 + \langle C\rangle_2 = 0$ at $t = 0$.

Reduction of the $\alpha-$integrals is accomplished as follows: if

$$I(t) = \int_0^\infty \frac{\mathrm{e}^{-t\alpha^2}}{\alpha^4 + \omega^2}\cos\lambda\alpha\,\mathrm{d}\alpha,$$

and $I(t)$ vanishes for $t \to \infty$, then

$$\frac{\mathrm{d}^2 I(t)}{\mathrm{d}t^2} + \omega^2 I(t) = \int_0^\infty \mathrm{e}^{-t\alpha^2}\cos\lambda\alpha\,\mathrm{d}\alpha = \frac{1}{2}\sqrt{\frac{\pi}{t}}\mathrm{e}^{-\lambda^2/4t}.$$

Let

$$I(t) = C_1(t)\,\mathrm{e}^{i\omega t} + C_2(t)\,\mathrm{e}^{-i\omega t}, \quad \text{with} \quad \mathring{C}_1(t)\mathrm{e}^{i\omega t} + \mathring{C}_2(t)\mathrm{e}^{-i\omega t} = 0.$$

Hence,

$$\frac{\mathrm{d}I(t)}{\mathrm{d}t} = i\omega\left[C_1(t)\mathrm{e}^{i\omega t} - C_2(t)\mathrm{e}^{-i\omega t}\right], \text{ and } \frac{\mathrm{d}^2 I(t)}{\mathrm{d}t^2} = i\omega\left[\mathring{C}_1(t)\mathrm{e}^{i\omega t} - \mathring{C}_2(t)\mathrm{e}^{-i\omega t}\right] - \omega^2\, I(t),$$

which means that

$$\mathring{C}_1(t)\mathrm{e}^{i\omega t} - \mathring{C}_2(t)\mathrm{e}^{-i\omega t} = \frac{1}{i\omega}\cdot\frac{1}{2}\sqrt{\frac{\pi}{t}}\,\mathrm{e}^{-\lambda^2/4t}.$$

Accordingly

$$\mathring{C}_1(t) = \frac{\mathrm{e}^{-\omega t}}{4i\omega}\sqrt{\frac{\pi}{t}}\,\mathrm{e}^{-\lambda^2/4t}, \quad \text{and} \quad \mathring{C}_2(t) = \frac{\mathrm{e}^{\omega t}}{4i\omega}\sqrt{\frac{\pi}{t}}\,\mathrm{e}^{-\lambda^2/4t},$$

that is

$$C_1(t) = \frac{i\sqrt{\pi}}{4\omega}\int_t^\infty \frac{\mathrm{e}^{-i\omega\tau}\mathrm{e}^{-\lambda^2/4\tau}}{\sqrt{\tau}}\mathrm{d}\tau, \quad \text{and} \quad C_2(t) = -\frac{i\sqrt{\pi}}{4\omega}\int_t^\infty \frac{\mathrm{e}^{i\omega\tau}\mathrm{e}^{-\lambda^2/4\tau}}{\sqrt{\tau}}\mathrm{d}\tau,$$

therefore

$$I(t) = \frac{\sqrt{\pi}}{2\omega}\int_t^\infty \frac{\sin\omega(\tau - t)}{\sqrt{\tau}}\,\mathrm{e}^{-\lambda^2/4\tau}\,\mathrm{d}\tau.$$

Checking the limit when $t \to 0$ it follows that

$$I(0) = \int_0^\infty \frac{\cos\lambda\alpha}{\alpha^4 + \omega^2}\,\mathrm{d}\alpha = \frac{\sqrt{\pi}}{2\omega}\int_t^\infty \frac{\sin\omega\tau}{\sqrt{\tau}}\,\mathrm{e}^{-\lambda^2/4\tau}\,\mathrm{d}\tau$$
$$= \frac{\sqrt{\pi}}{2\omega}\int_0^\infty \sin\omega x^2\,\mathrm{e}^{-\lambda^2/4x^2}\,\mathrm{d}x = \frac{\sqrt{\pi}}{2i\omega}\int_0^\infty \left\{\mathrm{e}^{i\omega x^2} - \mathrm{e}^{-i\omega x^2}\right\}\mathrm{e}^{-\lambda^2/4x^2}\mathrm{d}x.$$

Given that

$$\int_0^\infty \exp\left(-ax^2 - \frac{b}{x^2}\right)\,\mathrm{d}x = \frac{1}{2}\sqrt{\frac{\pi}{a}}\,\exp\left(-2\sqrt{ab}\right),$$

the previous integral becomes

$$\begin{aligned} I(0) &= \frac{\sqrt{\pi}}{2\,i\,\omega}\left\{\frac{1}{2}\sqrt{\frac{\pi}{\omega}}\,\mathrm{e}^{i\pi/4}\,\exp\left(-\frac{1-i}{\sqrt{2}}\lambda\sqrt{\omega}\right)\right. \\ &\qquad \left. -\frac{1}{2}\sqrt{\frac{\pi}{\omega}}\,\mathrm{e}^{-i\pi/4}\,\exp\left(-\frac{1+i}{\sqrt{2}}\lambda\sqrt{\omega}\right)\right\} \\ &= \frac{\pi}{2\,\omega^{3/2}}\,\exp\left(-\lambda\sqrt{\frac{\omega}{2}}\right)\,\sin\left(\frac{\pi}{4}+\lambda\sqrt{\frac{\omega}{2}}\right) \\ &= \frac{\pi}{2\sqrt{2}\,\omega^{3/2}}\,\exp\left(-\lambda\sqrt{\frac{\omega}{2}}\right)\left\{\cos\left(\lambda\sqrt{\frac{\omega}{2}}\right)+\sin\left(\lambda\sqrt{\frac{\omega}{2}}\right)\right\}, \end{aligned}$$

which agrees with the result

$$\int_0^\infty \frac{\cos ax}{x^4+b^2}\,\mathrm{d}x = \frac{\pi\sqrt{2}}{4b^3}\,\exp\left(-\frac{ab}{\sqrt{2}}\right)\,\left\{\cos\left(\frac{ab}{\sqrt{2}}\right)+\sin\left(\frac{ab}{\sqrt{2}}\right)\right\}.$$

Having in mind that

$$\begin{aligned} &\int_0^{\pi/2} \sin^2\varphi\,\mathrm{e}^{-\lambda\cos^2\varphi} = \int_0^{\pi/2}\frac{1-\cos 2\varphi}{2}\,\mathrm{e}^{-\frac{\lambda}{2}(1+\cos 2\varphi)}\,\mathrm{d}\varphi \\ &= \frac{1}{4}\int_0^{\pi}(1-\cos\psi)\,\mathrm{e}^{-\lambda/2}\cdot\mathrm{e}^{-\lambda/2\cos\psi}\,\mathrm{d}\psi = \frac{\pi}{4}\,\mathrm{e}^{-\lambda/2}\left\{I_0\Big(\frac{\lambda}{2}\Big)-I_1\Big(\frac{\lambda}{2}\Big)\right\}, \end{aligned}$$

so, $\langle C\rangle_2$ becomes

$$\langle C\rangle_2 = \frac{Q}{\sqrt{\pi D}}\int_t^\infty \frac{\sin\omega(\tau-t)}{\sqrt{\tau}}\Big\{1-\exp\Big(\frac{-a^2}{2D\tau}\Big)\Big[I_0\Big(\frac{a^2}{2D\tau}\Big)-I_1\Big(\frac{a^2}{2D\tau}\Big)\Big]\Big\}\mathrm{d}\tau.$$

Resolving the first integral therein,

$$\begin{aligned} I &= \int_t^\infty \frac{\sin\omega(\tau-t)}{\sqrt{\tau}}\,\mathrm{d}\tau = 2\cos\omega t\int_{\sqrt{t}}^\infty \sin\omega x^2\mathrm{d}x - 2\sin\omega t\int_{\sqrt{t}}^\infty \cos\omega x^2\mathrm{d}x \\ &= 2\sqrt{t}\,\cos\omega t\int_1^\infty \sin(\omega t\,\sigma^2)\,\mathrm{d}\sigma - 2\sqrt{t}\,\sin\omega t\int_1^\infty \cos(\omega t\,\sigma^2)\,\mathrm{d}\sigma \\ &= \frac{2}{\sqrt{\omega}}\,\cos\omega t\int_{\sqrt{\omega t}}^\infty \sin\mu^2\,\mathrm{d}\mu - \frac{2}{\sqrt{\omega}}\,\sin\omega t\int_{\sqrt{\omega t}}^\infty \cos\mu^2\,\mathrm{d}\mu, \qquad \omega\in\mathbb{R}\,. \end{aligned}$$

Recall the standard Fresnel integral definitions in un-normalized form:

$$S(x) = \int_0^x \sin t^2 \, \mathrm{d}t, \qquad C(x) = \int_0^x \cos t^2 \, \mathrm{d}t,$$

and note the standard limits

$$S(\infty) = C(\infty) = \frac{\sqrt{\pi}}{2\sqrt{2}}.$$

Note then that the last two integrals in I become

$$\int_{\sqrt{\omega t}}^{\infty} \sin \mu^2 \, \mathrm{d}\mu = \frac{\sqrt{\pi}}{2\sqrt{2}} - S\left(\sqrt{\omega t}\right), \qquad \int_{\sqrt{\omega t}}^{\infty} \cos \mu^2 \, \mathrm{d}\mu = \frac{\sqrt{\pi}}{2\sqrt{2}} - C\left(\sqrt{\omega t}\right).$$

whence

$$\begin{aligned} I &= \frac{2}{\sqrt{\omega}} \cos(\omega t)\Big[\frac{\sqrt{\pi}}{2\sqrt{2}} - S\left(\sqrt{\omega t}\right)\Big] - \frac{2}{\sqrt{\omega}} \sin(\omega t)\Big[\frac{\sqrt{\pi}}{2\sqrt{2}} - C\left(\sqrt{\omega t}\right)\Big] \\ &= \sqrt{\frac{\pi}{2\omega}} \cos(\omega t) - \frac{2}{\sqrt{\omega}} \cos(\omega t)\, S\left(\sqrt{\omega t}\right) - \sqrt{\frac{\pi}{2\omega}} \sin(\omega t) + \frac{2}{\sqrt{\omega}} \sin(\omega t)\, C\left(\sqrt{\omega t}\right) \\ &= \sqrt{\frac{\pi}{2\omega}} \left[\cos(\omega t) - \sin(\omega t)\right] + \frac{2}{\sqrt{\omega}} \left[\sin(\omega t)\, C\left(\sqrt{\omega t}\right) - \cos(\omega t)\, S\left(\sqrt{\omega t}\right)\right]. \end{aligned}$$

Finally,

$$\begin{aligned} \langle C\rangle_1 &= \frac{Q}{\sqrt{2D\omega}} \Bigg\{ \sin \omega t - \cos \omega t \\ &\qquad + \frac{4}{\pi} \Re\left[(1+i)\mathrm{e}^{i\omega t} \int_0^{\pi/2} \sin^2 \varphi \, \exp\left(-(1+i)a\sqrt{\frac{2\omega}{D}} \cos\varphi\right) \, \mathrm{d}\varphi\right]\Bigg\} \\ &= \frac{Q}{\sqrt{2D\omega}} \left\{ \sin \omega t - \cos \omega t - \Re\left[\mathrm{e}^{i\omega t} \frac{\mathbf{M}_1\left((1+i)a\sqrt{\frac{2\omega}{D}}\right)}{a\sqrt{\frac{2\omega}{D}}}\right]\right\}, \\ \langle C\rangle_2 &= \frac{Q}{\sqrt{\pi D}} \Bigg\{ \int_t^{\infty} \frac{\sin \omega(\tau - t)}{\sqrt{\tau}} \, \mathrm{d}\tau \\ &\qquad - \frac{4}{\pi} \int_0^{\pi/2} \sin^2 \varphi \int_t^{\infty} \frac{\sin \omega(\tau - t)}{\sqrt{\tau}} \, \exp\left(\frac{-a^2 \cos^2 \varphi}{D\tau}\right) \, \mathrm{d}\tau \, \mathrm{d}\varphi \Bigg\}, \\ &= \frac{Q}{\sqrt{2D\omega}} \left\{ \left[\cos(\omega t) - \sin(\omega t)\right] + \frac{2\sqrt{2}}{\sqrt{\pi}} \left[\sin(\omega t)\, C\left(\sqrt{\omega t}\right) - \cos(\omega t)\, S\left(\sqrt{\omega t}\right)\right]\right\} \\ &\qquad - \frac{Q}{\sqrt{\pi D}} \int_t^{\infty} \frac{\sin \omega(\tau - t)}{\sqrt{\tau}} \exp\left(\frac{-a^2}{2D\tau}\right) \left[I_0\Big(\frac{a^2}{2D\tau}\Big) - I_1\Big(\frac{a^2}{2D\tau}\Big)\right] \, \mathrm{d}\tau, \; \omega \in \mathbb{R}. \end{aligned}$$

It is worth showing the limiting behavior of $\langle C\rangle_2$ at short times. Consider again Equation (25) at its large-s asymptotic response. Note

$$\langle \bar{C}\rangle_2 = \frac{2Q\omega}{D(s^2+\omega^2)} \left\{ \frac{1}{2q} - \frac{2}{\pi q} \int_0^{\pi/2} \sin^2 \varphi \, e^{-2aq\cos\varphi} d\varphi \right\}, \qquad q = \sqrt{\frac{s}{D}}.$$

For large s, the integral term vanishes exponentially leaving:

$$\langle \bar{C} \rangle_2 \sim \frac{2Q\omega}{D(s^2+\omega^2)} \cdot \frac{1}{2q} \sim \frac{Q\omega}{D(s^2+\omega^2)} \cdot \sqrt{\frac{D}{s}}.$$

At large s, with all ω:

$$\langle \bar{C} \rangle_2 \sim \frac{Q\omega}{D} \cdot \frac{1}{s^2} \cdot s^{-1/2} = \frac{Q\omega}{D}\, s^{-5/2},$$

and with

$$\mathcal{L}^{-1}\left\{ \frac{1}{s^{5/2}} \right\} = \frac{4}{3\sqrt{\pi}}\, t^{3/2},$$

note the leading short-time behavior:

$$\langle C \rangle_2(t) \sim \frac{Q\omega}{D} \cdot \frac{4}{3\sqrt{\pi}}\, t^{3/2}.$$

Therefore:

$$\langle C \rangle_2 \propto t^{3/2} \propto (\omega t)^{3/2}, \qquad t \ll \frac{1}{\omega},\ t \ll \frac{a^2}{D}.$$

Conflicts of Interest. The authors declare that they have no conflicts of interest regarding the publication of this article.

References

[1] M. Fleischmann and S. Pons, The behavior of microdisk and microring electrodes. Mass transport to the disk in the unsteady state: the ac response, *J. Electroanal. Chem. Interfacial Electrochem.* **250** (1988) 277–283, https://doi.org/10.1016/0022-0728(88)85169-6.

[2] R. Ferrigno and H. H. Girault, Finite element simulation of electrochemical ac diffusional impedance. Application to recessed microdiscs, *J. Electroanal. Chem.* **492** (2000) 1–6, https://doi.org/10.1016/S0022-0728(00)00236-9.

[3] M. Saghafi, S. Chinnathambi and S. G. Lemay, High-frequency phenomena and electrochemical impedance spectroscopy at nanoelectrodes, *Curr. Opin. Colloid Interface Sci.* **63** (2023) #101654, https://doi.org/10.1016/j.cocis.2022.101654.

[4] L. M. Abrantes, M. Fleischmann, L. M. Peter, S. Pons and B. R. Scharifker, On the diffusional impedance of microdisc electrodes, *J. Electroanal. Chem. Interfacial Electrochem.* **256** (1988) 229–233, https://doi.org/10.1016/0022-0728(88)85023-X.

[5] K. Wheeler, J. Gott, B. Roehrich, J. Chung, K. Kajal, J. Syzdek, J. Hespanha and L. Sepunaru, Investigation of noise at a microelectrode during a faradaic reaction, *ACS Electrochem.* **1** (2025) 552–559, https://doi.org/10.1021/acselectrochem.4c00117.

[6] P. G. Bruce, A. Lisowska-Oleksiak, P. Los and C. A. Vincent, Electrochemical impedance spectroscopy at an ultramicroelectrode, *J. Electroanal. Chem.* **367** (1994) 279–283, https://doi.org/10.1016/0022-0728(94)03303-X.

[7] J. Navarro-Laboulais, J. J. Garcia-Jareño and F. Vicente, Kramers–Kronig transformation, dc behaviour and steady state response of the Warburg impedance for a disk electrode inlaid in an insulating surface, *J. Electroanal. Chem.* **536** (2002) 11–18, https://doi.org/10.1016/S0022-0728(02)01173-7.

[8] R. Michel, C. Montella, C. Verdier and J. Diard, Numerical computation of the Faradaic impedance of inlaid microdisk electrodes using a finite element method with anisotropic mesh adaptation, *Electrochim. Acta* **55** (2010) 6263–6273, https://doi.org/10.1016/j.electacta.2009.12.093.

[9] Z. A. Rotenberg, A. V. Drobinskii, V. P. Lukovtsev and N. S. Khozyainova, Features of the electrochemical impedance at microelectrodes, *Elektrokhimiya* **36** (2000) 996–1000.

[10] C. Montella, The impedance spectroscopy response for a reversible electrode reaction based on diffusion limited chronoamperometry at an inlaid disk electrode, *J. Electroanal. Chem.* **776** (2016) 180–187, https://doi.org/10.1016/10.1016/j.jelechem.2016.07.003.

[11] A. Lasia, *Electrochemical Impedance Spectroscopy and its Applications*, Springer New York, NY, 2014, https://doi.org/10.1007/978-1-4614-8933-7.

[12] C. Gabrielli, F. Huet, M. Keddam, P. Rousseau and V. Vivier, Scanning electrochemical microscopy imaging by means of high-frequency impedance measurements in feedback mode, *J. Phys. Chem. B* **108** (2004) 11620–11626, https://doi.org/10.1021/jp0496809.

[13] M. Fleischmann, J. Daschbach and S. Pons, The behaviour of microdisk and microring electrodes: Application of Neumann's integral theorem to the prediction of the steady state response of microdisks, *J. Electroanal. Chem. Interfacial Electrochem.* **263** (1989) 189–203, https://doi.org/10.1016/0022-0728(89)85094-6.

[14] M. Fleischmann, S. Pons and J. Daschbach, The ac impedance of spherical, cylindrical, disk, and ring microelectrodes, *J. Electroanal. Chem. Interfacial Electrochem.* **317** (1991) 1–26, https://doi.org/10.1016/0022-0728(91)85001-6.

[15] T. K. Pogány and S. Pons, On the structure of complex variable Struve and modified Struve function of the second kind, *J. Nepal Math. Soc.* **8** (2025) 89–94, https://doi.org/10.3126/jnms.v8i1.80225.

[16] M. A. Shpot and T. K. Pogány, Feynman integral in $\mathbb{R}^1 \oplus \mathbb{R}^m$ and complex expansion of ${}_2F_1$, Integral Transforms Spec. Funct. 27 (2016) 533–547.

[17] H. Levine, On the solution of an unsteady diffusion problem and its ultimate behaviour, *Quart. J. Mech. Appl. Math.* **40** (1987) 213–222, https://doi.org/10.1093/qjmam/40.2.213.

[18] F. W. Olver, D. W. Lozier, R. F. Boisvert and C. W. Clark, *NIST Handbook of Mathematical Functions*, Cambridge University Press, New York, NY, 2010.

[19] W. Pons and S. Pons, Average surface temperature over the circular disk heat source/sink embedded in an insulating boundary plane. Analytic solution, *C. r. Méc.* **351** (2023) 17–27, https://doi.org/10.5802/crmeca.158.

[20] F. G. Leppington, The transmission of randomly incident sound through an elastic panel, *Proc. Roy. Soc. London Ser. A* **426** (1989) 153-165, https://doi.org/10.1098/rspa.1989.0121.

[21] G. N. Watson, *A Treatise on the Theory of Bessel Functions*, Cambridge University Press, Cambridge, 1944.

[22] M. Fleischmann and S. Pons, The behaviour of microdisk and microring electrodes. Mass transport to the disk in the unsteady state. Chronopotentionetry, *J. Electroanal. Chem. Interfacial Electrochem.* **250** (1988) 257–267, https://doi.org/10.1016/0022-0728(88)85167-2.